Station spacing bounds the recovery of rainfall extremes by interpolation: an independent-network test with consequences for landslide thresholds

SungHyun Min

Jeonbuk National University, 567 Baekje-daero, Deokjin-gu, Jeonju 54896, Republic of Korea

dark7208@gmail.com

ORCID: https://orcid.org/0000-0003-0511-5491

Preprint statement

This is a non-peer-reviewed preprint submitted to EarthArXiv.

The manuscript has been submitted to Journal of Hydrology (Elsevier) for peer review on 6 September 2026. It has not been peer reviewed. Subsequent versions of this manuscript may have different content. If accepted, the final version of this manuscript will be available via the 'Peer-reviewed Publication DOI' link on this page; the authors welcome feedback in the meantime.

Data and code

All derived tables, the six experiment outputs, the radar extractions and the analysis scripts are deposited at Zenodo: https://doi.org/10.5281/zenodo.22443355. Every table and figure in this manuscript can be regenerated from the deposit by running a single script.

Competing interests

The author was previously employed by the National Institute of Forest Science, which produces the mountain meteorological observations and the gridded products evaluated here. The author declares no financial interest. The evaluation was conducted independently at Jeonbuk National University on publicly available data.

Correspondence: SungHyun Min, dark7208@gmail.com

Station spacing bounds the recovery of rainfall extremes by interpolation: an independent-network test with consequences for landslide thresholds

Abstract

Gridded rainfall products interpolated from gauge networks underpin landslide early warning, and a common view holds that their main deficiency in mountains is the omission of orographic enhancement. This study tests that view with an independent network: 464 mountain stations operated by the Korea Forest Service, which do not enter the operational grid of the Korea Meteorological Administration. Over five summers (2020–2024, 92,663 wet station-days after quality control), daily rainfall interpolated from the 615 meteorological-agency stations alone was compared with what the mountain stations measured. Three findings follow. First, summer daily rainfall showed no systematic dependence on elevation: the median elevation gradient within the mountain network was −0.05 to +0.10 mm per 100 m across the five years, and interpolation from the lowland network reproduced the day-to-day gradient in sign and magnitude. Second, interpolation attenuated extremes in proportion to their intensity, capturing 112% of 1–10 mm days but 75% of days above 200 mm; the operational configuration classified only 26% of 200-mm days as exceeding 200 mm. Third, this loss was not recoverable: terrain-weighted regression, a PRISM-type local regression and ordinary kriging performed no better than inverse-distance weighting, and quadrupling gauge density raised exceedance detection from 0.25 to 0.37. Forty-four percent of the mountain extremes had no gauge within 10 km that recorded a comparable total. Radar reflectivity confirmed that these extremes were spatially real. At 9,656 landslide sites the operational field placed 25% above 200 mm; adding the mountain network raised this to 49%. The deficiency of the gauge-interpolated field for landslide forecasting is the attenuation of extremes between gauges, which denser networks and better interpolators do not cure and which the inclusion of mountain observations partly does.

Keywords: rainfall interpolation; gauge network density; extreme precipitation; orographic enhancement; landslide early warning; independent validation; Korea

1. Introduction

Landslide early warning at national scale rests on rainfall thresholds, and rainfall thresholds are evaluated on gridded fields interpolated from gauge observations (Guzzetti et al., 2008; Segoni et al., 2018; Piciullo et al., 2018). The warning decision therefore depends on how faithfully the interpolated field represents rainfall at the sites where slopes fail, and in particular how faithfully it represents the extreme daily totals that trigger failure. Interpolation is a weighted average, and a weighted average cannot exceed the largest value among its inputs; any extreme that falls between gauges is attenuated by construction (Hofstra et al., 2010; Gervais et al., 2014). How large this attenuation is, and whether it can be reduced, are practical questions for any warning service that relies on a gauge-based grid.

The prevailing diagnosis of gridded rainfall in mountainous regions is different. It holds that precipitation increases with elevation, that gauge networks under-sample high terrain, and that the interpolated field consequently omits orographic enhancement (Daly et al., 1994, 2008; Roe, 2005; Houze, 2012). Terrain-aware interpolators were developed to correct this. PRISM regresses precipitation on elevation locally with weights for distance, elevation and slope facet (Daly et al., 1994), and its Korean adaptation, MK-PRISM, is applied in the national 1-km grid (Shin et al., 2008; Park and Kim, 2013; National Institute of Forest Science, 2025). The strength of orographic control, however, depends on time scale and rainfall type (Bárdossy and Pegram, 2013), and its presence in daily rainfall during the East Asian summer monsoon, when convective systems and typhoons dominate, has rarely been tested directly.

Testing it requires observations that did not enter the grid. Gridded products are usually validated by leave-one-out cross-validation on their own input stations, which measures accuracy where gauges stand and says little about accuracy between them (Hofstra et al., 2010; Daly, 2006). South Korea offers an unusual opportunity. The Korea Forest Service operates a network of 464 automatic mountain meteorological stations (AMOS), sited at a median elevation of 507 m and at a median distance of 7.9 km from the nearest Korea Meteorological Administration (KMA) station (National Institute of Forest Science, 2025). The KMA operational grid is interpolated from KMA stations alone. The mountain network is therefore an independent test set for exactly the terrain and exactly the extremes that matter for landslides.

2

This study asks three questions. First, how well does a field interpolated from the KMA network reproduce daily rainfall at the mountain stations, and does the error depend on elevation or on intensity? Second, is the loss recoverable by any of the three remedies commonly proposed — terrain correction, a better interpolator, or a denser network? Third, what does the loss amount to at the sites of recorded landslides? The answers are obtained from six experiments on the same five summers, the same stations and the same metrics, supplemented by weather radar for one season and applied to 9,656 landslide records.

2. Data and methods

2.1. Two networks

Interpolation used the KMA surface network: 95 synoptic stations (ASOS) and 520 automatic weather stations (AWS), 615 in total after removing one station with an invalid coordinate. Validation used the Korea Forest Service AMOS network, 463 stations after the same check. Daily precipitation for June to September 2020–2024 was taken from the daily station files distributed for both networks; the number of AMOS stations reporting rose from 314 in 2020 to 462 in 2023 as the network was completed. Station elevation was read from a national digital elevation model. The two networks differ in siting (Fig. 1): the median AMOS elevation is 507 m, and the median elevation of the KMA station nearest to each AMOS site is 149 m. The median distance from an AMOS site to its nearest KMA station is 7.4 km in the coordinate file used here and 7.87 km in the 313-station table published with the network (National Institute of Forest Science, 2025).

3

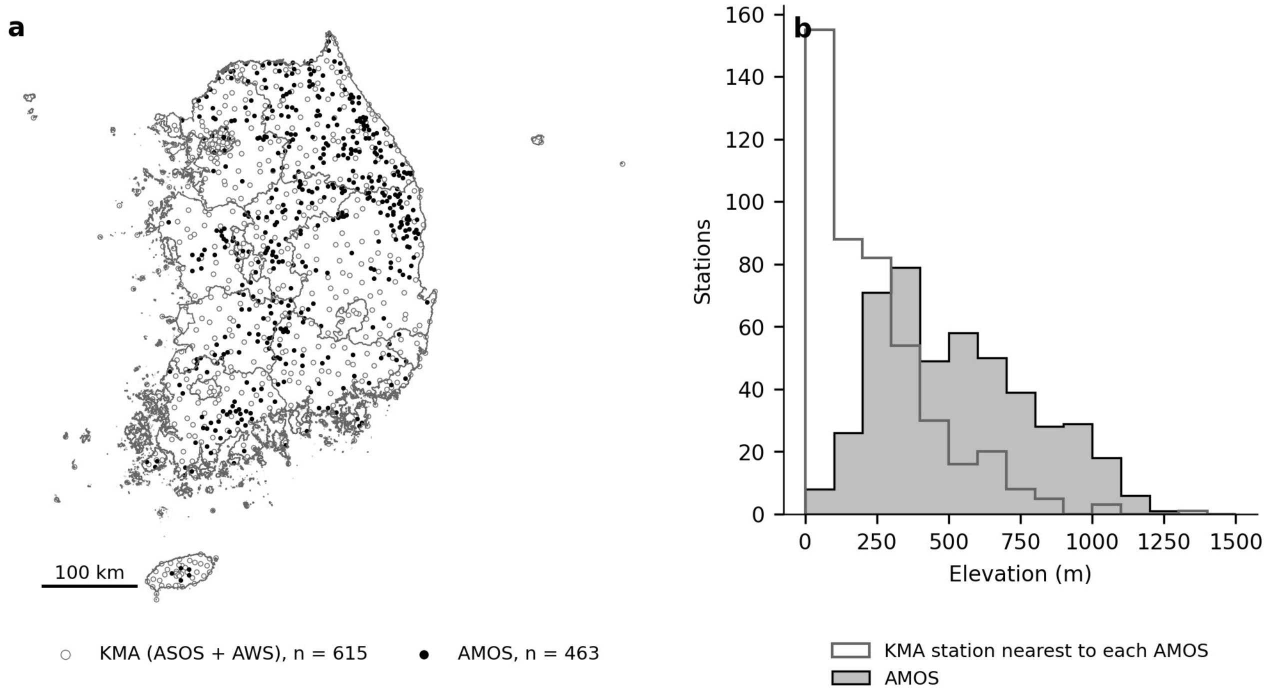

Fig. 1. The two networks. (a) KMA stations (open circles), which supply the interpolation, and AMOS stations (filled), which validate it. (b) Elevation of AMOS stations and of the KMA station nearest to each.

2.2. Quality control of the validation data

AMOS observations were removed if they reached the instrument ceiling (≥900 mm) or if they exceeded 200 mm on a day when the field interpolated from KMA stations within 60 km gave less than 2 mm at the site, a combination that cannot occur physically at daily scale. The rule removed 135 of the five-year station-days, 114 of them at the ceiling; 26 came from a single station and the count rose sharply in 2023–2024 when the network reached full size. Without the rule, root-mean-square error for 2024 was 62 mm; with it, 13 mm. The rule refers to the interpolated field only to identify dry surroundings and does not otherwise condition the validation on the field being tested.

2.3. Interpolators

All interpolators were run from the KMA stations to the AMOS locations on every day, so that every comparison uses the same days, inputs and targets. Inverse distance weighting (IDW) with power 2 and 12 neighbours within 60 km served as the reference; 60 neighbours approximates the operational configuration, which uses stations within a 60-km radius; 3 neighbours and power 4 were included as less smoothed variants. Nearest-station assignment, the largest station value within 10 km, and a blend

4

(the mean of IDW and the largest value within 15 km) represented extreme-preserving alternatives. Two terrain-aware methods were tested: a global regression of station rainfall on station elevation with IDW applied to the residuals, and a PRISM-type local regression in which stations within 50 km are weighted by inverse squared distance, by a Gaussian function of elevation difference (scale 300 m) and by cosine similarity of slope aspect (floor 0.2), and rainfall is regressed on elevation with those weights; the slope was clipped to −5 to +10 mm per 100 m, and targets with fewer than eight usable stations fell back to IDW. The operational MK-PRISM constants are not published; the structure implemented here is the documented one (Daly et al., 1994; Shin et al., 2008). Ordinary kriging used an exponential variogram fitted each day to the KMA station pairs by least squares, solved locally with 12 or 30 neighbours; on days too dry to fit a variogram the kriged value was replaced by IDW (Goovaerts, 2000).

2.4. Network density

To measure how extreme capture depends on gauge spacing, the KMA network was thinned at random to 25, 50 and 75% of its stations, three draws each, with the thinned set held fixed across all days. Each thinned network was interpolated to the AMOS sites and scored exactly as the full network. Density is reported as the median distance from an AMOS site to its nearest retained gauge, which rose from 7.3 km at full density to 14.3 km at 25%.

2.5. Metrics

Performance was evaluated on wet station-days (observed ≥ 1 mm) and stratified by observed intensity, by AMOS elevation and by distance to the nearest KMA station. The capture ratio is the mean predicted divided by the mean observed within a stratum. Threshold detection is the probability that the prediction exceeds a threshold given that the observation did,

(1)

for T = 100, 150 and 200 mm. False extremes are the fraction of days with observation below 30 mm on which the prediction exceeded 100 mm. Root-mean-square error and bias are reported for all wet pairs. The elevation gradient of rainfall on each day was estimated by regressing the AMOS observations on AMOS elevation, and separately by regressing the interpolated values on the same

5

elevations; the former is a property of the mountain network alone and the latter of the interpolated field.

2.6. Radar

KMA hybrid-surface-rainfall (HSR) reflectivity composites at 500 m and 5 min were obtained for 39 days of summer 2020 and read at the AMOS and KMA station cells. Reflectivity was converted to rain rate with a relation fitted to KMA's own point products (reflectivity and rain rate at 356 stations); the fit was weak (r = 0.68), consistent with the operational product using dual-polarisation estimation that a single Z–R relation cannot reproduce. Radar was therefore used only for a relative question: at an AMOS site where the gauge network missed an extreme, does the radar show more rain at that site than at the nearest KMA site? The ratio of the two radar accumulations is insensitive to the Z–R relation, which enters both. Radar was not used to estimate absolute totals; in this sample it captured about half of gauge totals above 200 mm, as is common for heavy rain (Krajewski and Smith, 2002; Berne and Krajewski, 2013).

2.7. Landslide sites

The Korea Forest Service landslide inventory supplies 9,656 point records for June 2020 to July 2023 (Korea Forest Service, 2023). The occurrence date in the inventory is the start date of the disaster event rather than the date of the individual failure: all 6,228 records of the July 2020 monsoon episode carry 28 July, although the rainfall that produced most of them fell in the first week of August. The analysis therefore uses event windows, from the recorded date to 5 days later for short events, 7 for typhoons, 10 for the July 2023 episode and 14 for the July 2020 episode, and takes the maximum daily and maximum three-day rainfall within the window at each site. Three fields were evaluated at every site: KMA stations only with 60 neighbours (the operational configuration), KMA stations only with the blend, and KMA and AMOS stations together with 12 neighbours. Each was also evaluated on a 5-km reference grid over land so that a site's rainfall could be ranked nationally for the same window.

Analysis scripts were drafted with the assistance of a large language model and verified against independently computed values; all analytical choices and interpretations are the author's. The scripts and all derived tables are deposited (Section 7).

3. Results

3.1. No systematic orographic enhancement

Within the mountain network, daily rainfall showed no consistent dependence on elevation. The median elevation gradient across wet days was −0.05 mm per 100 m in 2020, +0.04 in 2021, +0.08 in 2022, +0.10 in 2023 and +0.05 in 2024; the gradient was positive on 48–57% of days and the median correlation between rainfall and elevation across stations was −0.01. Mean daily rainfall on wet days declined slightly with elevation, from 24.4 mm below 200 m to 21.5 mm at 1,000–1,300 m. Typhoon days were the exception: Maysak and Haishen (2–3 and 7 September 2020) produced gradients of +3.7 to +5.8 mm per 100 m, whereas the heaviest convective days of July 2020 produced gradients of −1.0 to −2.7.

The field interpolated from KMA stations reproduced these gradients. On 7 September 2020 the AMOS network showed +5.80 mm per 100 m and the interpolated field +5.19; on 3 September +5.68 and +4.63; on 23 July −2.72 and −2.78. The lowland network, interpolated without any terrain term, followed the sign and magnitude of the day's elevation dependence. Whatever the interpolated field lacks at mountain sites, it is not the orographic gradient.

3.2. Interpolation attenuates extremes in proportion to intensity

Across 92,663 wet station-days, the capture ratio of IDW declined monotonically with observed intensity: 1.12 for 1–10 mm, 0.93 for 10–30, 0.90 for 30–50, 0.87 for 50–100, 0.84 for 100–150, 0.81 for 150–200 and 0.75 above 200 mm (Fig. 2). The pattern was stable across years: the ratio above 200 mm was 0.75, 0.85, 0.77, 0.72 and 0.73 for 2020 to 2024. Light rain is over-predicted and heavy rain under-predicted, which is the signature of a weighted average pulling every value toward its neighbours. Stratified by elevation the ratio fell from 0.95 below 200 m to 0.82 at 1,000–1,300 m, but the observed rainfall in those bands also fell, and the elevation dependence of the error is small compared with its intensity dependence.

The operational configuration, with 60 neighbours, lost more (Table 1). Its capture ratio above 200 mm was 0.70, and on the 408 station-days on which an AMOS station recorded 200 mm or more, the operational field exceeded 200 mm at that site on 26% of them. The corresponding figure for 150 mm was 0.44 and for 100 mm 0.55. Reducing the neighbourhood raised detection: 12 neighbours gave

0.37 at 200 mm, 3 neighbours 0.46, the nearest station 0.52. The extreme-preserving methods went further: the largest value within 10 km gave 0.56 and the blend 0.55, with root-mean-square error of 16.9 and 14.7 mm against 13.5 for IDW and with false extremes on 0.10% and 0.06% of light-rain days against 0.02%.

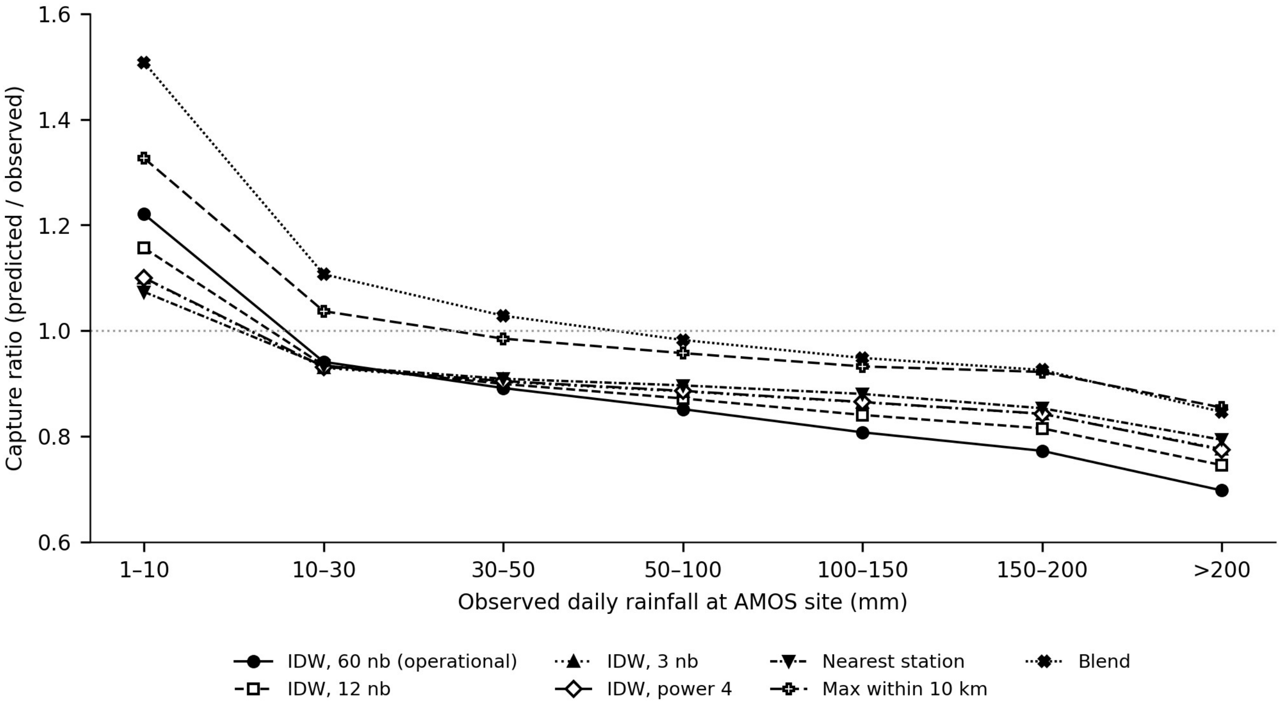

Fig. 2. Capture ratio (mean predicted / mean observed) at AMOS sites by observed daily intensity for seven interpolators run from KMA stations, 2020–2024 summers, 92,663 wet station-days.

Table 1. Performance of interpolators at AMOS sites on wet station-days, 2020–2024 summers.

Method	Capture >200	P(200)	P(150)	RMSE (mm)	False >100 (%)
IDW, 60 neighbours (operational)	0.70	0.26	0.44	14.0	0.02
IDW, 12 neighbours	0.75	0.37	0.54	13.5	0.02
IDW, 3 neighbours	0.78	0.46	0.60	13.7	0.03
Nearest station	0.79	0.52	0.63	15.7	0.05
Largest within 10 km	0.85	0.56	0.67	16.9	0.10
Blend	0.85	0.55	0.68	14.7	0.06
Ordinary kriging, 12 nb	0.75	0.38	0.53	13.6	0.02
Ordinary kriging, 30 nb	0.73	0.37	0.51	13.8	0.02
Global elevation regression	0.80	—	—	21.6	—
PRISM-type local regression	0.71	0.32	0.50	17.8	—

P(T) is the probability that the prediction exceeds T given that the observation did. False >100 is the share of days with observation below 30 mm on which the prediction exceeded 100 mm. The global regression row is for 2020 only.

8

3.3. Nearly half of the extremes lie between gauges

Of the 408 station-days with AMOS totals of 200 mm or more, 44% had no KMA station within 10 km that recorded 200 mm, and 11% had none that recorded half the AMOS total. For these days no interpolator can reach the observed value, because the value is absent from the inputs; the largest-within-10-km method, which assigns the highest nearby observation without averaging, is the ceiling of what the network can supply, and it reached 0.56. The exponential variograms fitted each day had a median range of 158 km and a nugget-to-sill ratio of 0.08, so the daily fields were spatially coherent at the synoptic scale and the kriging neighbourhood was well within the correlated range. The extremes that were missed are features below the scale that the station-to-station covariance describes.

3.4. Three remedies that do not work

Terrain correction made the field worse. The global elevation regression raised root-mean-square error from 16.1 to 21.6 mm in 2020 and over-predicted at high elevation, with a capture ratio of 1.28 at 1,000–1,300 m. The PRISM-type local regression raised error from 13.5 to 17.8 mm over the five years, over-predicted light rain by a factor of 1.56, and captured slightly less of the extremes than IDW (0.71 against 0.74). Its apparent improvement at elevation, a capture ratio of 0.97 at 1,000–1,300 m against 0.82 for IDW, sits on a general upward bias rather than on recovered extremes (Fig. 4). Both methods impose an elevation dependence that the data do not contain.

A better interpolator made no difference. Ordinary kriging with 12 or 30 neighbours matched IDW to within 0.01 in every intensity band, in threshold detection and in error (Table 1, Fig. 4). Kriging minimises expected squared error, which rewards smoothing; it has no mechanism for restoring a value absent from its inputs.

A denser network helped only slowly (Fig. 3). Thinning the KMA network to 25% raised the median gauge distance from 7.3 to 14.3 km and lowered detection at 200 mm from 0.37 to 0.25; restoring the full network recovered 0.37. Quadrupling station count thus gained 0.12 in detection, and a linear extension of the curve puts detection near 0.42 for a network of 1,200 stations at 5-km spacing. The blend followed a parallel curve from 0.32 to 0.55. No practical density on this curve reaches the fraction of extremes that the mountain network measured.

9

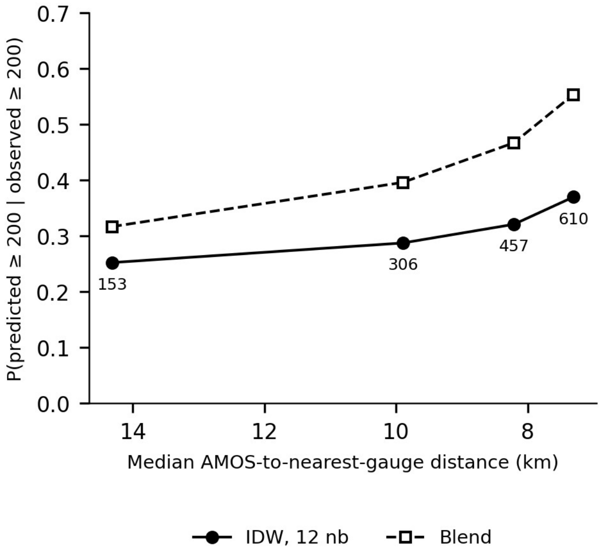

Fig. 3. Threshold detection at 200 mm as a function of gauge density, expressed as the median distance from an AMOS site to its nearest retained KMA gauge. Numbers give retained station count.

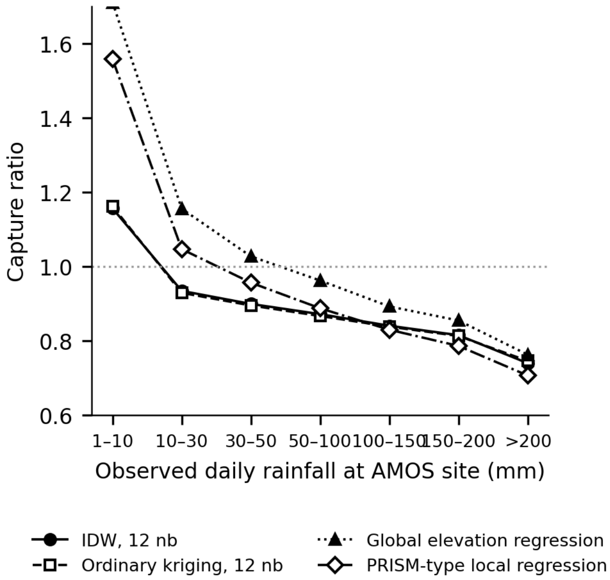

Fig. 4. Capture ratio by observed intensity for the four interpolator families. Kriging is indistinguishable from IDW; both terrain-aware methods over-predict light rain without recovering extremes.

3.5. Radar confirms the missed extremes

For the 39 radar days of summer 2020, the ratio of radar accumulation at the AMOS site to radar accumulation at the nearest KMA site was computed for every wet AMOS station-day (Fig. 5). For observed totals of 100–200 mm the median ratio was 1.04 and the AMOS site was wetter on 60% of days. For totals of 200 mm or more that the gauge network also saw, the ratio was 1.09 and 65%. For

10

the 33 days of 200 mm or more on which no KMA gauge within 10 km reached 200 mm, the ratio was 1.14 and the AMOS site was the wetter of the two on 94%. Where the gauge network missed an extreme, the radar placed the rain at the mountain site rather than at the gauge in 31 of 33 cases. The ratio is modest because radar also smooths and saturates in heavy rain; its consistency is the evidence. If these extremes were instrument artefacts the radar would show no preference.

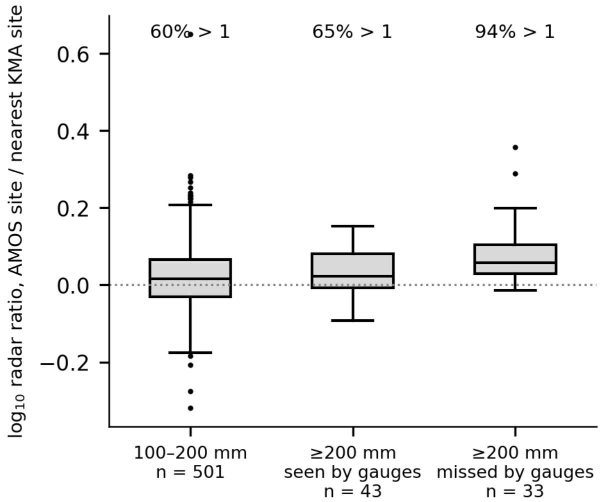

Fig. 5. Radar accumulation at the AMOS site relative to the nearest KMA site, 39 days of summer 2020, for three groups of AMOS observations. Percentages give the share of days on which the AMOS site was the wetter.

3.6. At landslide sites

Within the event windows, the landslide sites were among the wettest places in the country under every field: 80% of sites lay in the top quintile of the national maximum-daily field under the operational configuration and 84% under the two alternatives. Where the fields differed was in the level they assigned (Fig. 6). The median maximum daily rainfall at a landslide site was 165 mm under the operational field, 198 mm with AMOS included and 206 mm with the blend. The operational field placed 60% of sites above 150 mm and 25% above 200 mm; adding the AMOS stations raised these to 75% and 49%, and the blend to 82% and 54%. The AMOS field gave more rain than the operational field at 88% of sites, with a median ratio of 1.11, and 2,259 sites (23.6%) crossed 200 mm on the strength of the mountain stations alone. The three-day maxima told the same story at a higher level: 40% of sites above 300 mm under the operational field and 58% with AMOS.

11

By event (Fig. 7), the July–August 2020 monsoon episode moved from 62% of sites above 150 mm under the operational field to 79% with AMOS; Typhoons Maysak and Haishen from 49% to 62%, and to 80% with the blend. The blend over-reached in one setting: for the Seoul storm of August 2022, where the KMA network is dense, it placed 91% of sites above 150 mm against 47% for the AMOS field. It is a threshold-detection device, not a rainfall estimator, and its use should be confined to that role.

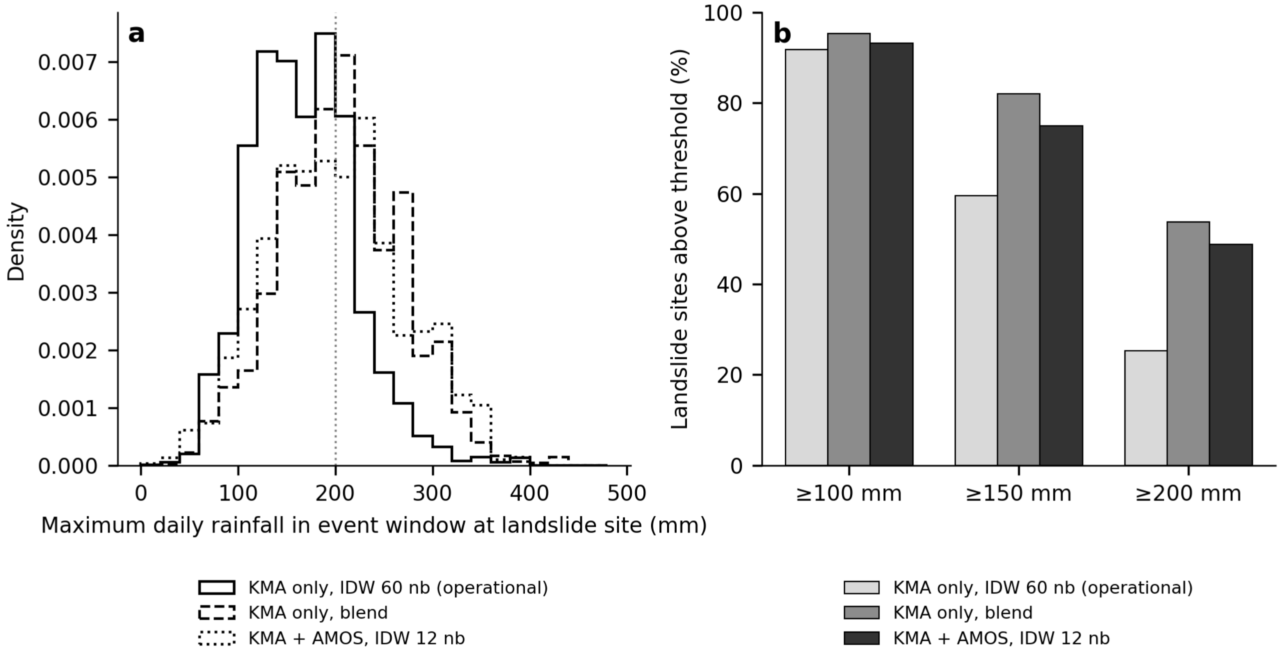

Fig. 6. Maximum daily rainfall in the event window at 9,656 landslide sites under three fields. (a) Distribution. (b) Share of sites above three thresholds.

12

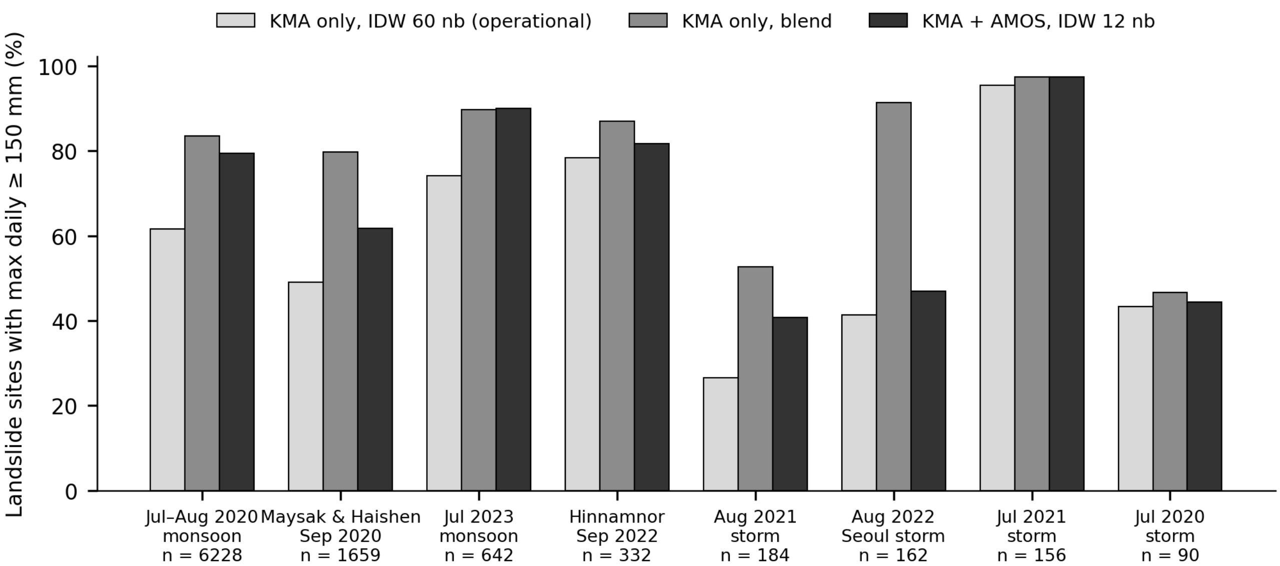

Fig. 7. Share of landslide sites with maximum daily rainfall of 150 mm or more, by event, under the three fields.

4. Discussion

4.1. The premise of orographic enhancement

The mountain network did not measure more rain than the lowland network on summer days. It measured slightly less. This does not contradict the physics of orographic precipitation, which is well established for stable flow over terrain (Roe, 2005; Houze, 2012) and which appeared clearly on the typhoon days of September 2020. It reflects the character of Korean summer rainfall, most of which arrives in convective systems along the monsoon front, where the location of a cell is set by mesoscale dynamics rather than by the slope beneath it. Bárdossy and Pegram (2013) showed that the topographic influence on precipitation weakens as the time scale shortens; the present result extends that to daily totals in a monsoon climate. Terrain correction applied without regard to rainfall type therefore imposes a dependence that is absent on most days and present on a few, and on average it adds error. The operational use of MK-PRISM (Shin et al., 2008) is not thereby shown to be wrong; it is shown to have a condition of application that summer daily rainfall does not meet.

4.2. Why the loss is not recoverable

Every interpolator tested is a weighted combination of the observed values, and no weighted combination can exceed the largest of them. When an extreme lies between gauges, the largest observed value is smaller than the extreme, and the interpolated value is smaller still. Kriging, which

13

minimises expected squared error, smooths at least as much as IDW; terrain regression can add to the estimate only if elevation carries information that the data show it does not. The one lever that can raise the input maximum is gauge density, and the density experiment shows how weak that lever is: a fourfold change in station count moved detection by 0.12. The horizontal scale of the missed extremes is smaller than the 7-km spacing of the present network, as the variogram range of 158 km shows in another way — the station-to-station covariance describes the synoptic field, not the cells embedded in it. Hofstra et al. (2010) and Gervais et al. (2014) reported the same intensity-dependent attenuation in European and North American gridded products; the present study measures it against an independent network in the terrain where it matters most.

4.3. What does work

Three conclusions for practice follow. First, mountain observations should enter the interpolation. The Korea Forest Service already does this in its own products; the present results quantify what it buys at the sites where landslides occur: a quarter of all sites crossing the 200-mm line that the KMA-only field placed them below. Second, threshold detection and rainfall estimation are different tasks and should use different fields. The blend detected 200-mm days twice as often as the operational configuration at a cost of 0.04% false extremes, but it over-estimated light rain by half and over-reached in dense urban networks; it belongs in the threshold-exceedance step of a warning chain and nowhere else. Third, the 44% of extremes that no gauge saw will require radar. Radar underestimates heavy rain and needs gauge adjustment (Kitchen and Blackall, 1992; Ciach and Krajewski, 1999; Sinclair and Pegram, 2005), but it resolves the horizontal scale that gauges do not, and in the present sample it located the missed extremes correctly in 31 of 33 cases. Quality control of the mountain data must precede all of this: the raw network contained ceiling and fault values that, uncorrected, quadrupled the validation error.

4.4. The landslide inventory

The inventory records the start date of a disaster event rather than the date of each failure. Evaluated on that date alone, the sites showed a median daily rainfall of 5 mm, because the rain had not yet arrived. The event-window analysis recovers the expected picture, with four-fifths of sites in the national top quintile, but the finding stands on its own: a rainfall-threshold analysis that takes the

14

inventory date at face value will conclude that landslides occur without rain. Recording the estimated time of failure alongside the damage report would remove the ambiguity, and would allow rainfall thresholds to be evaluated against the hours that actually preceded each failure rather than against a nominal event date.

4.5. Limitations

The analysis is at daily resolution, which is the resolution of the operational grid and of most landslide thresholds but not of convective rainfall; hourly data would sharpen the intensity dependence and might reveal orographic effects that daily totals average out. Radar covered one season and 39 days. The PRISM-type implementation uses conventional constants because the operational ones are unpublished, and omits a coastal term; since the elevation gradient it would exploit is absent, the constants are unlikely to change the result. The Z–R relation fitted to KMA's point products was weak, which is why radar was used relatively rather than absolutely. The mountain network expanded during the study period, so the 2020 results rest on 314 stations and the later years on 462.

5. Conclusions

Validated against 464 independent mountain stations over five summers, a daily rainfall field interpolated from the national meteorological network reproduced the elevation dependence of rainfall, which was small, and attenuated the extremes, which was not. The attenuation grew with intensity to a quarter of the total above 200 mm, and the operational configuration recognised only one in four such days as exceeding its own threshold. Terrain correction, kriging and a fourfold change in gauge density did not recover the loss, because 44% of the extremes had no gauge within 10 km that measured them; radar confirmed that they were real. At the sites of 9,656 landslides, including the mountain network in the interpolation doubled the share of sites above 200 mm. For landslide forecasting the question is not how to represent the mountains but how to keep the extremes, and the answer lies in the observations that enter the grid, not in the method that spreads them.

Declarations

Funding No funding was received for this study.
Declaration of competing interest The author was previously employed by the National Institute of Forest Science, which produces the mountain meteorological observations and the gridded products

15

discussed here. The author declares no financial interest. The evaluation was conducted independently at Jeonbuk National University on publicly available data.

Declaration of generative AI use During the preparation of this work the author used Claude (Anthropic) to draft analysis scripts and to assist with the English text. The author verified every script against independently computed values, reviewed and edited all text, and takes full responsibility for the content.

Supplementary material Supplementary material accompanying this article (Sections S1-S6) reports the elevation gradients by year, the year-by-year stability of extreme capture, the quality-control removals, the individual thinning draws, the fitted variograms and the Z-R calibration.

Data availability All derived tables, the seven experiment outputs, the radar extractions and the analysis scripts are deposited at Zenodo, https://doi.org/10.5281/zenodo.22443355. Daily station files are distributed by the Korea Meteorological Administration and the Korea Forest Service; radar composites by the KMA API Hub.

CRediT SungHyun Min: conceptualization, methodology, software, validation, formal analysis, data curation, writing – original draft, writing – review and editing, visualization.

References

Bárdossy, A., Pegram, G., 2013. Interpolation of precipitation under topographic influence at different time scales. Water Resour. Res. 49, 4545–4565. https://doi.org/10.1002/wrcr.20307

Berne, A., Krajewski, W.F., 2013. Radar for hydrology: unfulfilled promise or unrecognized potential? Adv. Water Resour. 51, 357–366. https://doi.org/10.1016/j.advwatres.2012.05.005

Ciach, G.J., Krajewski, W.F., 1999. On the estimation of radar rainfall error variance. Adv. Water Resour. 22, 585–595. https://doi.org/10.1016/S0309-1708(98)00043-8

Daly, C., 2006. Guidelines for assessing the suitability of spatial climate data sets. Int. J. Climatol. 26, 707–721. https://doi.org/10.1002/joc.1322

Daly, C., Neilson, R.P., Phillips, D.L., 1994. A statistical-topographic model for mapping climatological precipitation over mountainous terrain. J. Appl. Meteorol. 33, 140–158. https://doi.org/10.1175/1520-0450(1994)033<0140:ASTMFM>2.0.CO;2

Daly, C., Halbleib, M., Smith, J.I., Gibson, W.P., Doggett, M.K., Taylor, G.H., Curtis, J., Pasteris, P.P., 2008. Physiographically sensitive mapping of climatological temperature and precipitation across the conterminous United States. Int. J. Climatol. 28, 2031–2064. https://doi.org/10.1002/joc.1688

Dirks, K.N., Hay, J.E., Stow, C.D., Harris, D., 1998. High-resolution studies of rainfall on Norfolk Island. Part II: interpolation of rainfall data. J. Hydrol. 208, 187–193. https://doi.org/10.1016/S0022-1694(98)00155-3

Gervais, M., Tremblay, L.B., Gyakum, J.R., Atallah, E., 2014. Representing extremes in a daily gridded precipitation analysis over the United States: impacts of station density, resolution, and gridding methods. J. Clim. 27, 5201–5218. https://doi.org/10.1175/JCLI-D-13-00319.1

Goovaerts, P., 2000. Geostatistical approaches for incorporating elevation into the spatial interpolation of rainfall. J. Hydrol. 228, 113–129. https://doi.org/10.1016/S0022-1694(00)00144-X

Guzzetti, F., Peruccacci, S., Rossi, M., Stark, C.P., 2008. The rainfall intensity–duration control of shallow landslides and debris flows: an update. Landslides 5, 3–17. https://doi.org/10.1007/s10346-007-0112-1

16

Haylock, M.R., Hofstra, N., Klein Tank, A.M.G., Klok, E.J., Jones, P.D., New, M., 2008. A European daily high-resolution gridded data set of surface temperature and precipitation for 1950–2006. J. Geophys. Res. 113, D20119. https://doi.org/10.1029/2008JD010201

Hofstra, N., New, M., McSweeney, C., 2010. The influence of interpolation and station network density on the distributions and trends of climate variables in gridded daily data. Clim. Dyn. 35, 841–858. https://doi.org/10.1007/s00382-009-0698-1

Houze, R.A., 2012. Orographic effects on precipitating clouds. Rev. Geophys. 50, RG1001. https://doi.org/10.1029/2011RG000365

Kidd, C., Becker, A., Huffman, G.J., Muller, C.L., Joe, P., Skofronick-Jackson, G., Kirschbaum, D.B., 2017. So, how much of the Earth's surface is covered by rain gauges? Bull. Am. Meteorol. Soc. 98, 69–78. https://doi.org/10.1175/BAMS-D-14-00283.1

Kitchen, M., Blackall, R.M., 1992. Representativeness errors in comparisons between radar and gauge measurements of rainfall. J. Hydrol. 134, 13–33. https://doi.org/10.1016/0022-1694(92)90026-R

Korea Forest Service, 2023. Development of integrated landslide hazard forecasting technology. Research Report 23-02, National Institute of Forest Science, Seoul (in Korean).

Krajewski, W.F., Smith, J.A., 2002. Radar hydrology: rainfall estimation. Adv. Water Resour. 25, 1387–1394. https://doi.org/10.1016/S0309-1708(02)00062-3

Ly, S., Charles, C., Degré, A., 2013. Different methods for spatial interpolation of rainfall data for operational hydrology and hydrological modeling at watershed scale: a review. Biotechnol. Agron. Soc. Environ. 17, 392–406.

Marshall, J.S., Palmer, W.M., 1948. The distribution of raindrops with size. J. Meteorol. 5, 165–166. https://doi.org/10.1175/1520-0469(1948)005<0165:TDORWS>2.0.CO;2

National Institute of Forest Science, 2025. Development of a mountain-area impact forecasting base and a customized mountain meteorology and climate service system. Research Report 25-01, Seoul (in Korean).

Park, J.C., Kim, M.K., 2013. Comparison of precipitation distributions in precipitation data sets representing 1 km spatial resolution over South Korea produced by PRISM, IDW, and cokriging. J. Korean Assoc. Geogr. Inf. Stud. 16, 147–163. https://doi.org/10.11108/kagis.2013.16.3.147 (in Korean with English abstract).

Piciullo, L., Calvello, M., Cepeda, J.M., 2018. Territorial early warning systems for rainfall-induced landslides. Earth-Sci. Rev. 179, 228–247. https://doi.org/10.1016/j.earscirev.2018.02.013

Roe, G.H., 2005. Orographic precipitation. Annu. Rev. Earth Planet. Sci. 33, 645–671. https://doi.org/10.1146/annurev.earth.33.092203.122541

Segoni, S., Piciullo, L., Gariano, S.L., 2018. A review of the recent literature on rainfall thresholds for landslide occurrence. Landslides 15, 1483–1501. https://doi.org/10.1007/s10346-018-0966-4

Shin, S.C., Kim, M.K., Suh, M.S., Rha, D.K., Jang, D.H., Kim, C.S., Lee, W.S., Kim, Y.H., 2008. Estimation of high resolution gridded precipitation using GIS and PRISM. Atmosphere (Korean Meteorol. Soc.) 18, 71–81 (in Korean with English abstract).

Sinclair, S., Pegram, G., 2005. Combining radar and rain gauge rainfall estimates using conditional merging. Atmos. Sci. Lett. 6, 19–22. https://doi.org/10.1002/asl.85

Villarini, G., Mandapaka, P.V., Krajewski, W.F., Moore, R.J., 2008. Rainfall and sampling uncertainties: a rain gauge perspective. J. Geophys. Res. 113, D11102. https://doi.org/10.1029/2007JD009214

17

Supplementary material

Station spacing bounds the recovery of rainfall extremes by interpolation: an independent-network test with consequences for landslide thresholds

SungHyun Min, Jeonbuk National University. Journal of Hydrology.

Contents: S1 elevation gradients by year; S2 year-by-year stability of extreme capture; S3 quality-control removals; S4 individual draws of the network-thinning experiment; S5 fitted variograms; S6 the Z–R calibration. Numerical values are also supplied in the data deposit (https://doi.org/10.5281/zenodo.22443355).

S1 Elevation gradient of daily rainfall, by year

Section 3.1 reports the median elevation gradient of daily rainfall within the AMOS network for each summer. Fig. S1 gives the full distribution. The gradient is computed for every day on which the network mean exceeded 1 mm and at least 50 stations reported, by regressing station rainfall on station elevation. The distributions are centred on zero in every year, with interquartile ranges of roughly ±0.5 mm per 100 m and long tails on both sides; the positive tail contains the typhoon days discussed in Section 3.1 and the negative tail the convective episodes.

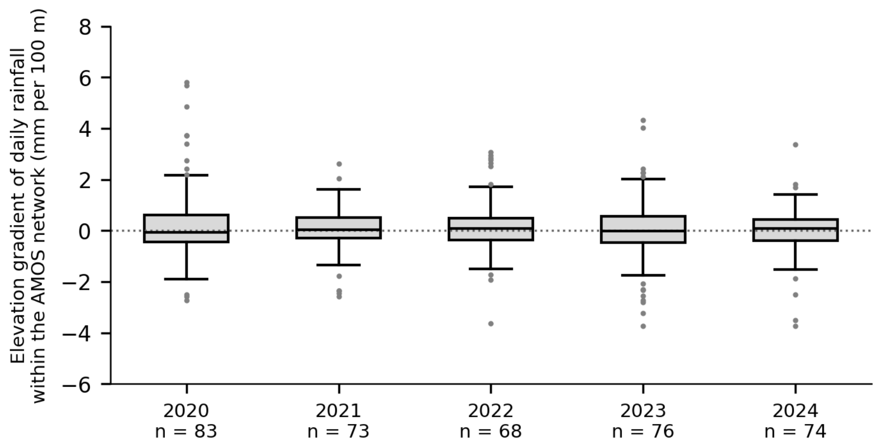

Fig. S1. Daily elevation gradient of rainfall within the AMOS network, by year. Boxes give the interquartile range, whiskers 1.5 times that range, points the remainder.

Table S1. Elevation gradient of daily rainfall within the AMOS network, by year.

Year	Days	Median (mm/100 m)	IQR (mm/100 m)	Positive (%)	AMOS stations
2020	83	−0.05	−0.43 to +0.61	48	314
2021	73	+0.04	−0.28 to +0.52	55	364
2022	68	+0.08	−0.36 to +0.48	57	413
2023	76	−0.01	−0.46 to +0.55	49	462
2024	74	+0.08	−0.40 to +0.43	57	462

Days with network mean rainfall of at least 1 mm and at least 50 reporting stations.

S2 Year-by-year stability of extreme capture

The intensity-dependent attenuation reported in Section 3.2 is a five-year average. Fig. S2 shows that it is present in every year and that the ordering of methods does not change, although the level does.

Capture above 200 mm was highest in 2021 and lowest in 2023 and 2024. The number of station-days above 200 mm varies by a factor of four between years, from 33 in 2021 to 138 in 2023, so the 2021 point rests on the fewest cases. The operational configuration was the weakest method in every year.

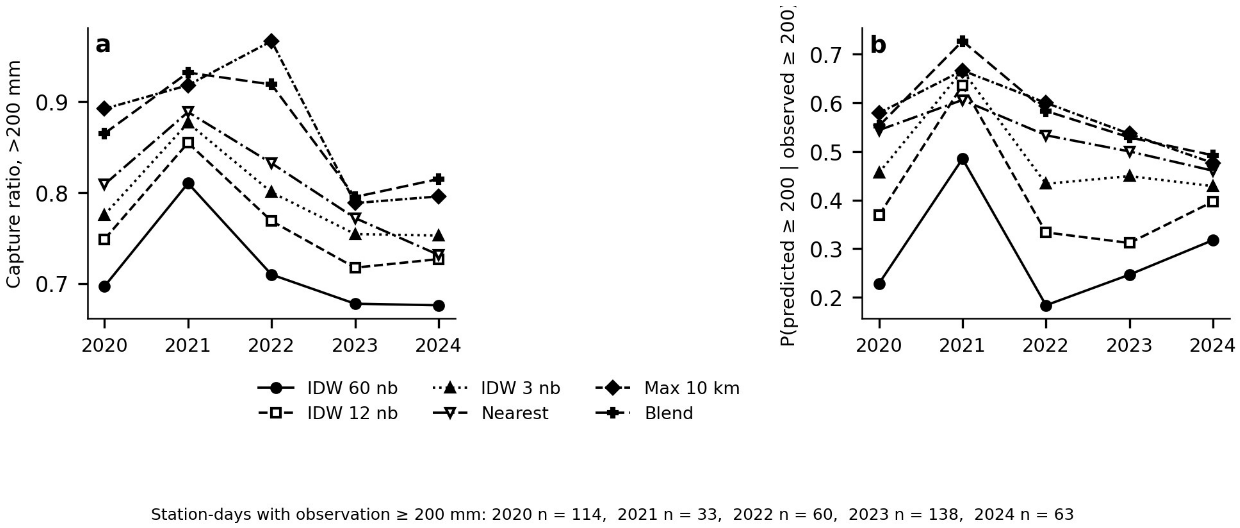

Fig. S2. Capture of extremes by year and method. (a) Capture ratio for observations above 200 mm. (b) Probability that the prediction exceeds 200 mm given that the observation did.

S3 Quality-control removals

The rule described in Section 2.2 removed 135 station-days from the five-year record: 114 at or above the instrument ceiling of 900 mm and 21 reporting 200 mm or more on days when the surrounding gauges were dry. Removals are not evenly distributed. One station accounts for 26 of them, the ten most affected stations for 102, and the count rises with the size of the reporting network: one removal in 2020, 48 in 2023 and 86 in 2024. Reported values cluster tightly just below 1,000 mm, the signature of a saturating counter rather than of rainfall (Fig. S3b). Without the rule, root-mean-square error for 2024 rises from 13 to 62 mm.

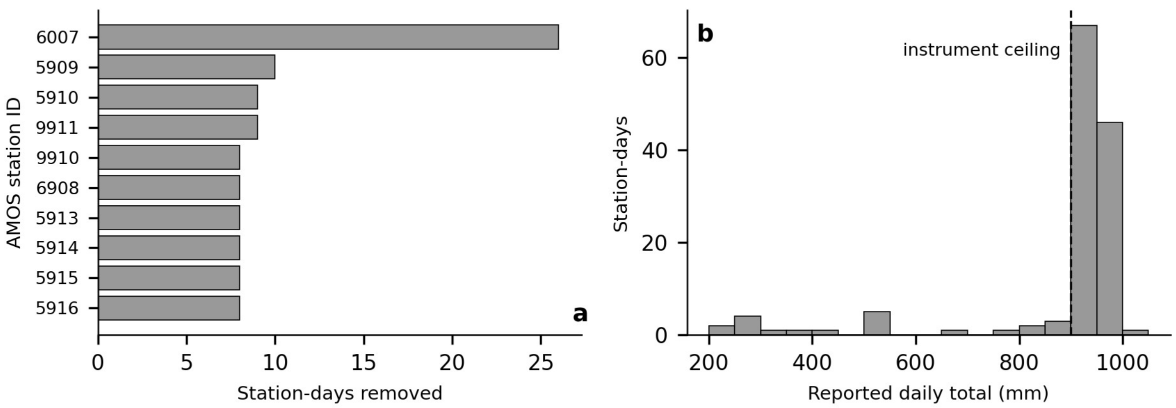

Fig. S3. Quality-control removals. (a) The ten AMOS stations with the most removed station-days. (b) Distribution of the removed values; the dashed line marks the 900 mm instrument ceiling.

S4 Individual draws of the network-thinning experiment

Each thinning fraction in Section 3.4 was drawn three times, with the retained set held fixed across all 610 days. Table S2 gives the individual draws. Variation between draws at the same fraction is 0.01 to 0.03 in threshold detection, an order of magnitude smaller than the change between fractions, so the density curve of Fig. 3 is not an artefact of any single draw.

Table S2. Threshold detection at 200 mm for each thinning draw.

Fraction	Draw	KMA stations	IDW, 12 nb	Blend
0.25	1	153	0.272	0.343
0.25	2	152	0.245	0.328
0.25	3	154	0.240	0.279
0.50	1	306	0.279	0.407
0.50	2	306	0.299	0.377
0.50	3	306	0.284	0.404
0.75	1	458	0.333	0.488
0.75	2	458	0.321	0.451
0.75	3	457	0.309	0.463
1.00	—	610	0.370	0.554

S5 Fitted variograms

Exponential variograms were fitted to the KMA station pairs on each of the 503 days with enough rain to define one. The median range is 158 km, but the distribution is bimodal (Fig. S5a): a mode near 40–100 km on days with organised convection, and a large group at the upper bound of the fitting window on days when the field is spatially uniform and the variogram does not reach a sill within the 150 km search. The nugget-to-sill ratio has a median of 0.085, and is below 0.1 on 41% of days, indicating that station-to-station variation at short lags is small relative to the total. Both properties place the kriging neighbourhood well inside the correlated range, which is why kriging behaves like inverse-distance weighting: the field it interpolates is smooth at the scale it can see.

The median gauge spacing of 7.4 km, marked in Fig. S5a, lies below almost every fitted range. The extremes that the network misses are therefore not resolved by the covariance structure that kriging estimates, which describes the synoptic field rather than the cells embedded in it.

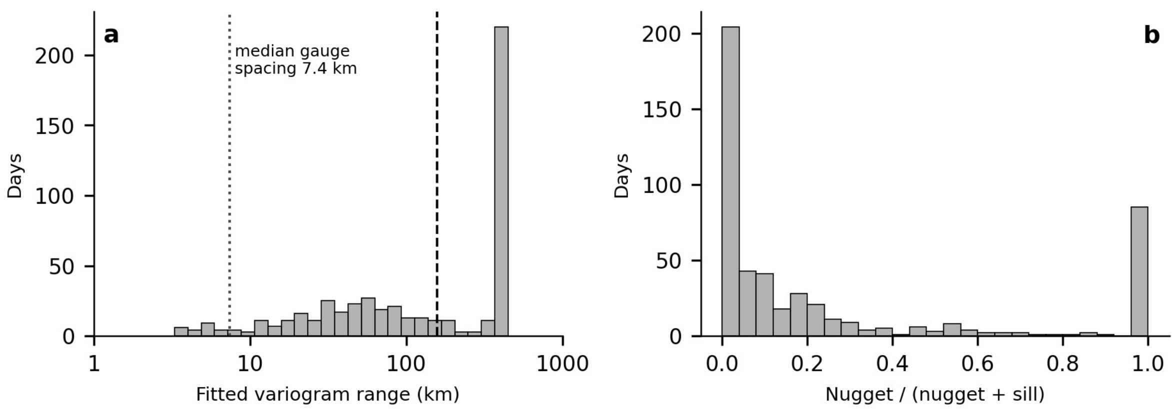

Fig. S5. Daily variograms fitted to the KMA stations. (a) Fitted range; dashed line, the median of 158 km; dotted line, the median gauge spacing of 7.4 km. (b) Nugget as a fraction of the total sill.

S6 The Z–R calibration

Radar reflectivity was converted to rain rate using a relation fitted to KMA's own point products: the reflectivity (HSR) and the rain rate (HSP) reported at the same 356 stations and the same instants. Five rainy times supplied 255 usable pairs with reflectivity above 5 dBZ and rain rate above 0.1 mm per hour. Least squares on log rain rate gives log10 R = −0.723 + 0.0441 dBZ, equivalent to Z = 44 R^2.27, against the Marshall–Palmer values of 200 and 1.6.

The fit is weak, with a correlation of 0.68 on log rain rate and an interquartile ratio of predicted to reported rate of 0.4 to 1.7 for the Marshall–Palmer form. At a given reflectivity the reported rate spans two orders of magnitude (Fig. S6). This is expected: the operational product uses dual-polarisation variables that a single reflectivity-to-rate relation cannot reproduce. It is the reason radar is used in Section 3.5 only through the ratio of two accumulations computed with the same relation, in which the relation cancels, and not to estimate rainfall amounts.

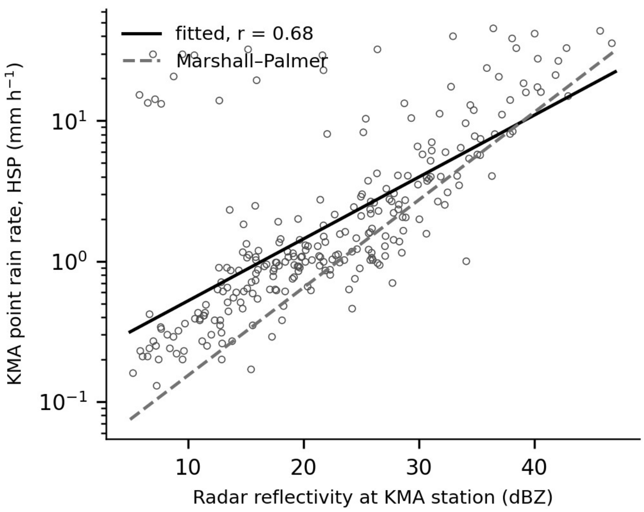

Fig. S6. Radar reflectivity against KMA's reported rain rate at the same stations and instants, 255 pairs from five rainy times. Solid line, the fitted relation; dashed line, Marshall–Palmer.